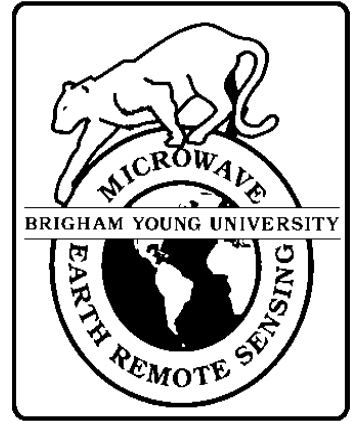




**Brigham Young University  
Department of Electrical and  
Computer Engineering**

**459 Clyde Building  
Provo, Utah 84602**



# **Azimuthal Modulation of Ku-Band Scatterometer Sigma-0 Over the Antarctic**

**Quinn P. Remund  
David S. Early  
David G. Long, Ph.D.**

**3 July 1997**

**MERS Technical Report # MERS 97-02  
ECEN Department Report # TR-L110-97.2**

---

**Microwave Earth Remote Sensing (MERS)  
Laboratory**

© Copyright 1997, Brigham Young University. All rights reserved.

# Azimuthal Modulation of Ku-Band Scatterometer $\sigma^o$ Over the Antarctic

Quinn P. Remund, David S. Early, and David G. Long  
Brigham Young University

July 3, 1997

## Abstract

The azimuthal modulation characteristics of Antarctic sea ice are evaluated using techniques developed by David S. Early for the ERS-1 AMI scatterometer. Azimuthal modulation can produce adverse affects in a number of applications including resolution enhancement through image reconstruction techniques. Several regions of sea ice and glacial ice are selected for the experiment. Incidence angle dependence is assessed and minimized through limiting the range of angles used and through fore-aft beam differencing. Plots of  $\sigma^o$  vs. azimuth angle are used to identify regions with azimuthal modulation. The fore-aft beam  $\sigma^o$  difference is also used as an indicator of azimuthal modulation. This study concludes that azimuthal modulation in all sea ice regions observed was less than 0.6 dB while much higher values were observed in glacial ice regions. It should be noted that this study was conducted before the final calibration of NSCAT was complete. As a result, it is expected that some bias is present in the results which could reduce modulation.

## 1 Introduction

Historically, space-borne scatterometers have been employed primarily in atmospheric and oceanic studies. Rapid repeat coverage makes these instruments valuable in these applications. The low nominal spatial resolution inherent to scatterometers is acceptable for studying such large scale phenomenon. Spaceborne scatterometers have also been used to study non-ocean surface parameters (e.g. [1] [2] [3] [4] [5]). However, for land and ice studies, this low resolution presents a problem.

The SIRF algorithm was developed [6] to enhance scatterometer image resolution by combining data from multiple passes of the satellite. The method was originally created for studies in the Amazon region where azimuthal modulation is minimal [1]. Figure 1 illustrates a SIRF  $\mathcal{A}$  value image of Antarctica for 1996 JD 259-264. An exceptional amount of detail is visible in this and other similar NSCAT images. This information can be utilized in surface parameter extraction studies.

This paper will examine the azimuthal modulation characteristics of Antarctic sea and glacial ice to determine the applicability of this image reconstruction algorithm to the Southern Ocean region of the earth. Section 2 discusses characteristics of ice types in the Antarctic and how these characteristics contribute to the level of azimuthal modulation. Section 3 describes the analysis process using two methods to detect azimuthal modulation. Section 4 contains the conclusions drawn from this study.

## 2 Antarctic Ice Characteristics

The Antarctic is a region of diverse ice types and characteristics. The sea ice pack fluctuates in an oscillating seasonal cycle. During the winter freeze up, the ice pack thickens and grows outward. Antarctic summer causes the ice to recede toward the continent. The ice pack itself is composed of several different ice types. Nilas, first-year ice, multi-year ice, and icebergs are examples. Continental Antarctica also consists of different ice types such as glacial ice and is much less dynamic in its nature.

### 2.1 Surface Characteristics

In general, the Antarctic ice pack can be divided into two regimes: an outer ice pack and an inner ice pack, and for this study we use the definitions of these regimes as presented in [7]. Each regime has distinct physical properties that modulate microwave signatures of the ice as described below. The outer ice regime has two distinct phases: one during the winter freeze up and another during the summer melt.

The outer ice regime consists of the Marginal Ice Zone (MIZ) which is the extreme edge of the sea ice pack with a seasonally dependent makeup consisting of sea ice floes (up to several meters) surrounded by open water or slush [7]. The first phase of the outer ice regime occurs during early winter through early spring, when thermodynamic growth causes a rapid advance of the sea ice pack. The outer ice pack, and particularly the MIZ, are by definition regions of unconsolidated or uncoalesced ice during winter freeze up, so wave action in this region makes pancake ice predominant in early winter [8] [9]. A photograph of pancake ice taken at the edge of the ice pack is shown in Fig. 2 and illustrates the development of pancake ice in the outer ice regime. Oscillatory wave action pushes grease ice, new ice and slush together and eventually thermodynamic cooling causes the pancakes to solidify. Before pancake ice fields coalesce, the spaces surrounding the pancakes are either open water, frazil or grease ice. Thermodynamic effects will eventually cause the pancake field to coalesce into a solid ice pack. The second phase of the outer ice zone occurs during the spring and summer melt and break up of the sea ice pack. With the spring and summer warming, the pack ice begins to break up and melt, resulting in the MIZ containing large volumes of small, broken floes and brash ice.

The inner ice pack is typically thin to thick first year ice. Evidence from passive microwave systems shows that multiyear ice can survive in the Antarctic and it tends to be concentrated in the western Weddell Sea along the eastern edge of the Antarctic Peninsula [10]. Ridging, a major contributor to large scale deformation in Arctic sea ice, is in general much less intense in the Antarctic than in the Arctic with a lower average ridge height and lower frequency in the main body of the sea-ice pack [11] [12]. Also, as the ice ages, floes in the pack can be laden with snow to cause a negative freeboard condition, flooding the snow-ice interface. The existence of this wet slush layer changes the microwave properties of the sea ice, as does the subsequent re-freezing of this slush layer [4].

### 2.2 Azimuthal Modulation in the Antarctic

Azimuthal modulation of  $\sigma^o$  has been observed over the Antarctic ice sheet. Using Ku-Band SEASAT scatterometer data, *Remy et al.* [13] demonstrated that observed

azimuthal modulation over the Antarctic ice sheet is related to the katabatic winds on the continent. Further, any oriented scatterers, including sastrugi, wind oriented drifts and crevasse fields, may create azimuthal modulation in the satellite data. Ice sheets, even without significant oriented scatterers on the surface, can create azimuth modulation if there is a significant surface slope (e.g. a glacier in a mountain valley).

Sea ice, on the other hand, has much different surface characteristics than land ice sheets. Small scale waves such as millimeter, capillary or gravity waves are absent in the outer ice regime and the rest of the sea-ice pack because of the presence on the ocean surface of either solidified pack ice, pancake ice in its various forms or grease ice which prevent the formation of these small scale waves, eliminating one source of oriented scatterers in the ice pack. Also, the presence of water in the upper snow layer in some areas of the sea ice pack will change the structure of wind-etched surface features such as sastrugi. To further reduce the effects of any oriented scatterers that do develop on the sea ice surface, the dynamic motion of the ice surface causes a randomization of the scatterers over a large scale reducing the cumulative affect of scatterers on the return signal.

Since the sea ice floats on the surface of the ocean, we expect no inherent large scale surface slope associated with sea ice that would induce azimuthal modulation. However, because the ice in the outer ice regime is defined as uncoalesced ice, long wavelength swell-waves are capable of traveling through these outer regions of the sea ice pack [14] and inducing some surface slope. In the Southern Ocean, long wavelength swell waves, with wavelengths of several hundred meters and amplitudes of up to several meters are capable of traveling hundreds of kilometers into the sea-ice pack through pancake ice regions (M. Drinkwater, personal communication). Once the pancakes have begun to coalesce and solidify however, the waves are quickly damped out by the increasingly rigid sea-ice pack.

In the absence of significant wave action, any significant slope in the sea ice must result from ridging or stacking of ice floes. However, the divergent nature of the sea-ice pack causes break up, rotation and refreezing of sections of the ice which effectively randomizes small scale ridges and other oriented scatterers may form on the surface of the sea ice. This study concentrates on microwave scattering characteristics of Antarctic sea ice on the scale of the NSCAT scatterometer (25-50km), and we postulate that over the majority of the sea ice pack, relatively small structure variations in the sea-ice surface will not introduce substantial azimuthal variation in the scatterometer data due to the randomizing effects of the sea-ice pack motion.

Azimuthal modulation is undesirable in applications that require multiple passes of the satellite over a region. Azimuthal modulation means that  $\sigma^o$  is a function of azimuth angle. Over a limited  $\theta$  range of  $[20^\circ, 55^\circ]$ ,  $\sigma^o$  is approximately a linear function of  $\theta$ ,

$$\sigma^o(\theta) = \mathcal{A} + \mathcal{B}(\theta - 40^\circ)$$

where  $\mathcal{A}$  and  $\mathcal{B}$  are functions of surface characteristics, azimuth angle, and polarization.  $\mathcal{A}$  is the  $\sigma^o$  value at  $40^\circ$  incidence and  $\mathcal{B}$  describes the dependence of  $\sigma^o$  on  $\theta$ .  $\mathcal{A}$  and  $\mathcal{B}$  provide valuable information about surface parameters.  $40^\circ$  was chosen as a mid-swath value, but any interior swath angle will work.

## 3 Analysis

### 3.1 Removal of Incidence Angle Dependence

The study regions used in this project are identical to the regions used by David Early in his dissertation where he conducted a similar experiment with ERS-1 data. A description of these regions is given in Table 4. He chose the regions in a manner to ensure that they had little temporal variation and were spatially homogeneous. Twenty regions were chosen in the sea ice areas of Antarctica while five were chosen from the land ice and glacier areas. It is predicted that little azimuthal modulation will occur over sea ice and more will occur over the glacial ice.

This portion of the study was performed to determine if azimuthal modulation is incidence angle dependent. If there is no incidence angle dependency, then one incidence angle range can be used for the rest of the study. If this dependency does exist, representative ranges of incidence angles will need to be used in the study for the different swath regions (near, mid, and far).

For this project, 5 degree wide incidence angle ranges were used. The following are the ranges: 20-25, 25-30, 35-40, 40-45, 45-50, 55-60. For each of the ranges (for a given region) a histogram of record azimuth angles was produced to determine if there is enough azimuth angle diversity in the sampled data. Also, a  $\sigma^o$  time history was plotted to evaluate temporal dependencies. The mean and standard deviation of this history were computed. Finally, a scatterplot of  $\sigma^o$  versus azimuth angle was plotted to visually detect any azimuthal modulation.

Figure 3 illustrates an example of these plots for sea region I1 for the incidence angle range  $[40^\circ - 45^\circ]$ . The histogram demonstrates that the measurements for this region have good azimuth angle diversity. The time plot supports the argument that this region is relatively temporally invariant. Finally, the  $\sigma^o$  versus azimuth angle plot shows that there is little variation of  $\sigma^o$  with azimuth angle and thus little azimuth modulation. In contrast, Figure 4 shows the same plots for region G2 - a glacial region. Again, there is good azimuth angle diversity. However, azimuth modulation is observed since  $\sigma^o$  is clearly a function of azimuth angle. A difference of 5 dB in  $\sigma^o$  is observed at different angles. While these are only sample plots, a comprehensive set for all of the regions is contained in Appendix A.

The number of records, mean, and standard deviations of all the regions were plotted as a function of incidence angle as shown in Figures 5-9. Invariably the incidence angle range of 40-45 degrees had the most records and the most azimuth angle diversity. This suggests that these incidence angle ranges are the best to use for the study since we can get the most  $\sigma^o$  samples in the shortest amount of time. Of course, the study of an exclusive range of incidence angles can only be done if we find that there is little or no incidence angle dependence in the azimuthal modulation.

The plots also showed that the  $\sigma^o$  time history mean for each region was nearly linearly dependent on incidence angle with higher incidence angles yielding lower  $\sigma^o$ . For sea ice, the slope of the lines was nearly always the same for different regions - just shifted up or down from one another. The glacial regions had less constant slope as different regions were observed. Also, the slopes were flatter in general than the sea ice regions.

The standard deviations of the data from each region and at each range of incidence

angles seemed to be relatively flat. That is, as incidence angle changed the standard deviation was somewhat constant normally keeping within a .5 dB range (between max std and min std). If the standard deviation is any indication of azimuthal modulation, this would suggest that azimuthal modulation is not incidence angle dependent. However, this metric does not provide conclusive results about azimuthal modulation dependence on incidence angle. Thus, a more in depth study must be done by manually interpreting the data for each region and at each incidence angle.

### 3.2 Ku-Band $\sigma^o$ vs. Azimuth Angle

The  $\sigma^o$  vs. azimuth angle scatterplots described above give a good visual indication of azimuthal modulation. If the  $\sigma^o$  values aren't basically constant throughout the azimuth angles, modulation exists to some degree. As a metric of this phenomenon, the mean of every  $\sigma^o$  within 5 degree azimuth bins was computed and plotted over the top of the scatterplot. The range (max - min) of this curve should give a rough indication of how much  $\sigma^o$  changes through the possible range of azimuth angles. This range was computed for each region and each incidence angle range and plotted for each of these ranges. Two factors must be considered in the interpretation of the range plots. First, the overall levels of the curves which is an indication of the level of azimuthal modulation present. Second, the amount of change in the range as incidence angle is changes. This latter consideration will reveal any incidence angle dependence of the azimuthal modulation.

The range metric vs. incidence angle plots for each region is given in Figures 10-11. As shown in the plots, the sea ice regions have relatively low ranges (from about 1 to 5 dB) when compared with some of the glacial regions. The latter has a range from around 1 to 15 dB. This leads to the conclusion that less azimuthal modulation occurs for sea ice than for some glacial regions. However, it still seems that a significant amount of azimuthal modulation is occurring in the sea ice areas. While most of the regions had mean ranges around 2 or 3 this is still a significant amount of change in  $\sigma^o$ .

The mean  $\sigma^o$  range metric can be used to draw a second conclusion about azimuthal modulation - azimuthal modulation has low dependence on incidence angle. This is due to the fact that the range parameter changes only slightly with incidence angle for all observed regions (about 1-2 dB). Most regions followed the general trend of constant range in the near and mid swath (20-45 deg) and gradual increase in the far swath (45-60 deg) suggesting a slightly more azimuthal modulation at the higher incidence angles.

### 3.3 Fore-Aft Difference Analysis

The next step in the project was to investigate the fore-aft difference in  $\sigma^o$  values. Since the fore and aft beams are about 90 degrees offset in azimuth angle from one another, taking the difference between fore beam cells and aft beam cells in the same surface region and at the same incidence angle should give a good indication of azimuthal modulation. The observed  $\sigma^o$  can be viewed as the sum of a signal random variable with a noise random variable having a zero mean Gaussian distribution. The difference between the fore and aft beam measurements may be modeled by:

$$D = (\sigma_F^o + N_F) - (\sigma_A^o + N_A) \quad (1)$$

where  $N_F$  and  $N_A$  are independent Gaussian noise terms associated with the fore and aft beam measurements, respectively. We can predict  $D$  over an azimuthally isotropic medium. For an azimuthally isotropic medium,  $\sigma_F^o - \sigma_A^o = 0$  since the incidence angles for each measurement are equal, and  $D$  becomes the difference of the noise terms:

$$D = N_F - N_A. \quad (2)$$

When the difference is taken over an area with no azimuthal modulation (identical  $\sigma^o$  signal random variable values) the signal terms cancel one another and the difference in noise terms remains. Since the difference of two Gaussian random variables is a Gaussian random variable, we conclude that in regions with no azimuthal modulation the distribution of the fore-aft  $\sigma^o$  difference will be zero mean Gaussian.

Appendix B contains plots for each region of 1) a histogram of the difference measurement azimuth angles, 2) a histogram of fore-aft difference values, and 3) a scatterplot of the fore-aft difference vs. azimuth angle. For the Fore-aft difference histogram, a Gaussian distribution (dotted line) with the same mean and variance was also plotted. Samples of these plots are shown in Figures 12 and ?? for regions I2 and G2 respectively. I2 is a sea ice region while G2 is a glacial ice region.

An observation of the histograms for all the regions reveals that for the sea ice regions, the distributions are almost invariably near zero mean Gaussian as predicted. This indicates the absence of significant azimuth modulation in the backscatter signatures of these regions. For each of these fore-aft histograms, the mean and standard deviation is given at the top of the plots. With only two exceptions, the mean of these distributions for every regions was below .6 dB. We conclude from this that less than .6 dB of azimuthal modulation occurs in the sea ice regions of Antarctica. The non-zero mean may result from two sources. First, it may be caused by a low level of azimuthal modulation. Second, it may be an artifact of the incomplete calibration of the NSCAT data at the time of this study. Without proper beam balancing some bias will appear in the fore-aft difference. It is expected that after the data is processed with the correct calibration factors, the results will be more accurate. Regardless, this study demonstrates low azimuthal modulation in the sea ice areas.

An observation of similar plots of the glacial ice regions reveals some interesting features. Two of the five regions have distributions very similar to the characteristic sea ice distribution. That is, nearly zero mean Gaussian indicating low azimuthal modulation. The other regions have bimodal distributions leading to the conclusion that in the difference the signal terms do not cancel one another and more than just noise remains. We conclude from this that these areas have microwave properties conducive to azimuthal modulation in the backscatter signatures.

## 4 Conclusion

From this study we conclude that little azimuthal modulation (less than 1 dB) occurs in the sea ice regions of Antarctica for NSCAT scatterometer data. Some glacial regions exhibit a significant level of modulation in the data. These results support those of Early's ERS-1 C-Band study. Two methods were used to assess the level of azimuthal modulation for a given region. The first technique observed variations in  $\sigma^o$  vs. azimuth angle. Azimuthal modulation appears as changes in  $\sigma^o$  levels at different azimuth angles.

The second involved an analysis of the fore-aft beam difference. The distribution of the difference reveals the level of azimuthal modulation. The conclusion that can be drawn from this experiment is that azimuthal modulation can be neglected for sea ice for NSCAT data. That is, modulation in these regions will not significantly affect applications that require isotropic responses such as resolution enhancement.

## References

- [1] D. G. Long and P. J. Hardin, “Vegetation Studies of the Amazon Basin Using Enhanced Resolution Seasat Scatterometer Data”, *IEEE Transactions on Geoscience and Remote Sensing*, vol. 32, pp. 449–460, 1994.
- [2] D. Long and M. Drinkwater, “Greenland Ice-Sheet Surface Properties Observed by the Seasat-A Scatterometer at Enhanced Resolution”, *Journal of Glaciology*, vol. 40, no. 135, pp. 213–230, 1994.
- [3] M. Drinkwater, D. Long, and D. Early, “Enhanced Resolution ERS-1 Scatterometer Imaging of Southern Ocean Sea Ice”, *ESA Journal*, vol. 17, pp. 307–322, 1993.
- [4] A. R. Hosseinmostafa, V. I. Lytle, K. C. Jezek, S. P. Gogineni, S. F. Ackley, and R. K. Moore, “Comparison of Radar Backscatter from Antarctic and Arctic Sea Ice”, *Journal of Electromagnetic Waves and Applications*, vol. 9, no. 3, pp. 421–438, 1995.
- [5] P. Lecomte, A. Cavanie, and F. Gohin, “Recognition of Sea Ice Zones using ERS-1 Scatterometer Data”, in *Proceedings of IGARSS 93*. IEEE, 1993, pp. 855–857.
- [6] D. Long, P. Hardin, and P. Whiting, “Resolution Enhancement of Spaceborne Scatterometer Data”, *IEEE Transactions on Geoscience and Remote Sensing*, vol. 31, pp. 700–715, 1993.
- [7] J. Comiso, T. Grenfell, M. Lange, A. Lohanick, R. Moore, and P. Wadhams, “Microwave Remote Sensing of the Southern Ocean Ice Cover”, in *Microwave Remote Sensing of Sea Ice*, F. D. Carsey, Ed., chapter 12. American Geophysical Union, Boston, 1992.
- [8] M. A. Lange, S. F. Ackley, P. Wadhams, G. S. Diekmann, and H. Eicken, “Development of Sea Ice in the Weddell Sea”, *Annals of Glaciology*, , no. 12, pp. 92–96, 1991.
- [9] M. R. Drinkwater and C. Haas, “Snow, Sea-ice, and Radar Observations During ANT X/4: Summary Data Report”, Tech. Rep. 53, Alfred Wegener Institut, July 1994.
- [10] P. Gloersen, W. J. Campbell, D. J. Cavalieri, J. C. Comiso, C. L. Parkinson, and H. J. Zwally, *Arctic and Antarctic Sea Ice, 1978–1987: Satellite Passive–Microwave Observations and Analysis*, NASA, Washington, D.C., 1992.
- [11] V. I. Lytle and S. F. Ackley, “Sea Ice Ridging in the Eastern Weddell Sea”, *Journal of Geophysical Research*, vol. 96, no. 10, pp. 18411–18416, 1991.
- [12] W. Dierking, “Laser Profiling of the Ice Surface Topography During the Winter Weddell Gyre Study 1992”, *Journal of Geophysical Research*, vol. 100, no. C3, pp. 4807–4820, 1995.
- [13] F. Remy, Ledroit, and J. F. Minster, “Katabatic Wind Intensity and Direction over Antarctica Derived from Scatterometer Data”, *Geophysical Research Letters*, vol. 19, pp. 1021–1024, 1992.

- [14] A. K. Liu and S. Häkkinen, “Wave Effects on Ocean-Ice Interaction in the Marginal Ice Zone”, *Journal of Geophysical Research*, vol. 98, no. C6, pp. 10025–10036, 1993.

Tables

File Name	lon	lat	deg lon	deg lat	Julian Days	Mean	Std Dev
I1	312°	-75°	8°	4°	320-330	-14.93	0.773
I2	308°	-68°	10°	4°	320-330	-13.39	2.29
I3	0°	-70°	14°	3°	320-330	-16.97	2.32
I4	200°	-76°	10°	2°	320-330	-15.87	1.41
I5	196°	-74°	8°	4°	320-330	-15.77	1.54
I6	70°	-68°	8°	3°	320-330	-16.86	2.72
I7	192°	-73°	18°	5°	320-330	-15.70	1.61
I8	324°	-72°	10°	4°	320-330	-15.08	0.904
I10	322°	-76°	8°	3°	320-330	-15.79	1.95
I11	318°	-76°	8°	3°	320-330	-14.32	1.91
I12	314°	-76°	8°	3°	320-330	-13.93	1.91
I13	310°	-76°	8°	3°	320-330	-14.70	1.704
I14	306°	-76°	8°	3°	320-330	-15.31	1.01
I15	302°	-76°	8°	3°	320-330	-15.02	2.45
I16	322°	-73°	8°	3°	320-330	-14.72	0.79
I17	318°	-73°	8°	3°	320-330	-14.77	0.84
I18	314°	-73°	8°	3°	320-330	-15.25	0.88
I19	310°	-73°	8°	3°	320-330	-15.53	0.92
I20	306°	-73°	8°	3°	320-330	-15.90	1.16
I21	302°	-73°	8°	3°	320-330	-16.70	1.11
G1	140°	-78°	10°	2°	320-330	-4.03	0.90
G2	120°	-72°	10°	2°	320-330	-13.66	2.25
G3	40°	-74°	10°	2°	320-330	-7.25	1.91
G4	40°	-78°	10°	2°	320-330	-7.37	0.76
G5	80°	-72°	10°	2°	320-330	-12.09	3.35

## Figures

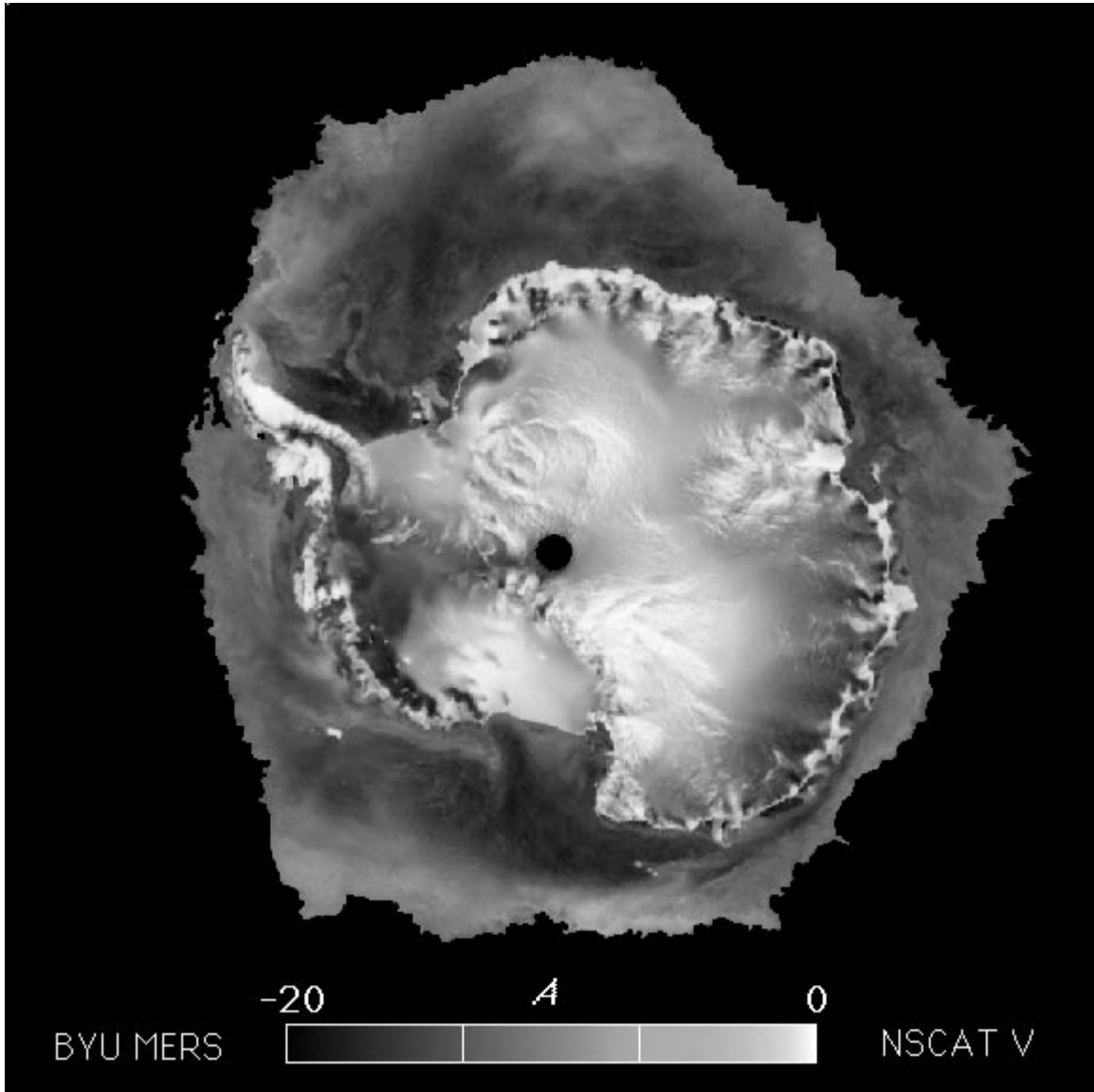


Figure 1: A polar stereographic projection image of Antarctica. The image is generated from 6 days of NSCAT data from JD 259 to JD 264 1996. An ice mask has been applied to the image.



Figure 2: Photograph of pancake ice taken near the Antarctic ice pack edge. Note the edges on the pancakes which are formed by wind and wave action forcing pancakes together and piling up the edge. Courtesy of Dr. Mark Drinkwater, JPL.

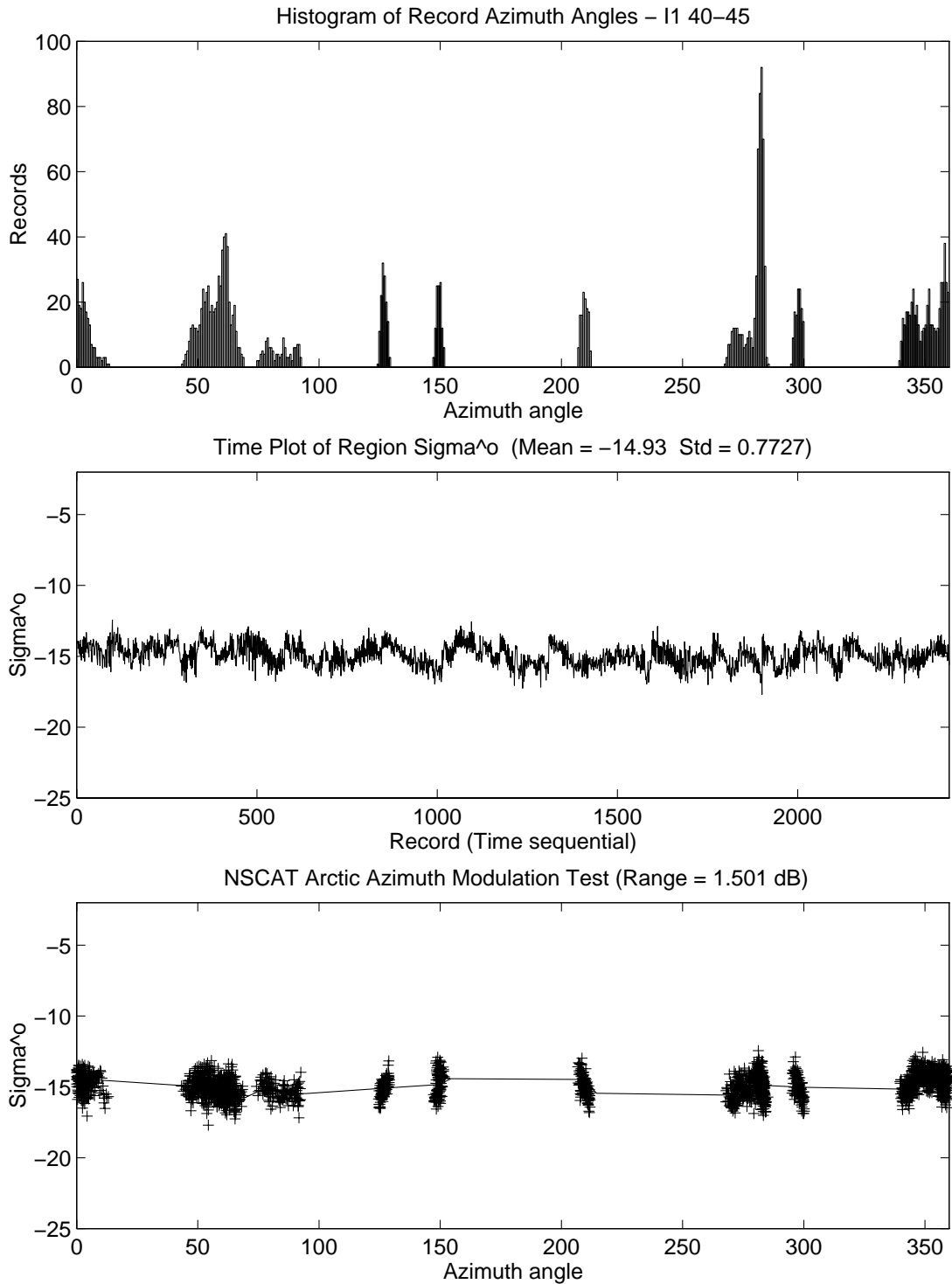


Figure 3: Plots illustrating the azimuth angle diversity,  $\sigma^o$  temporal dependence, and  $\sigma^o$  vs. azimuth angle for sea ice region I1. All measurements have incidence angles in the range  $[40^\circ - 45^\circ]$ .

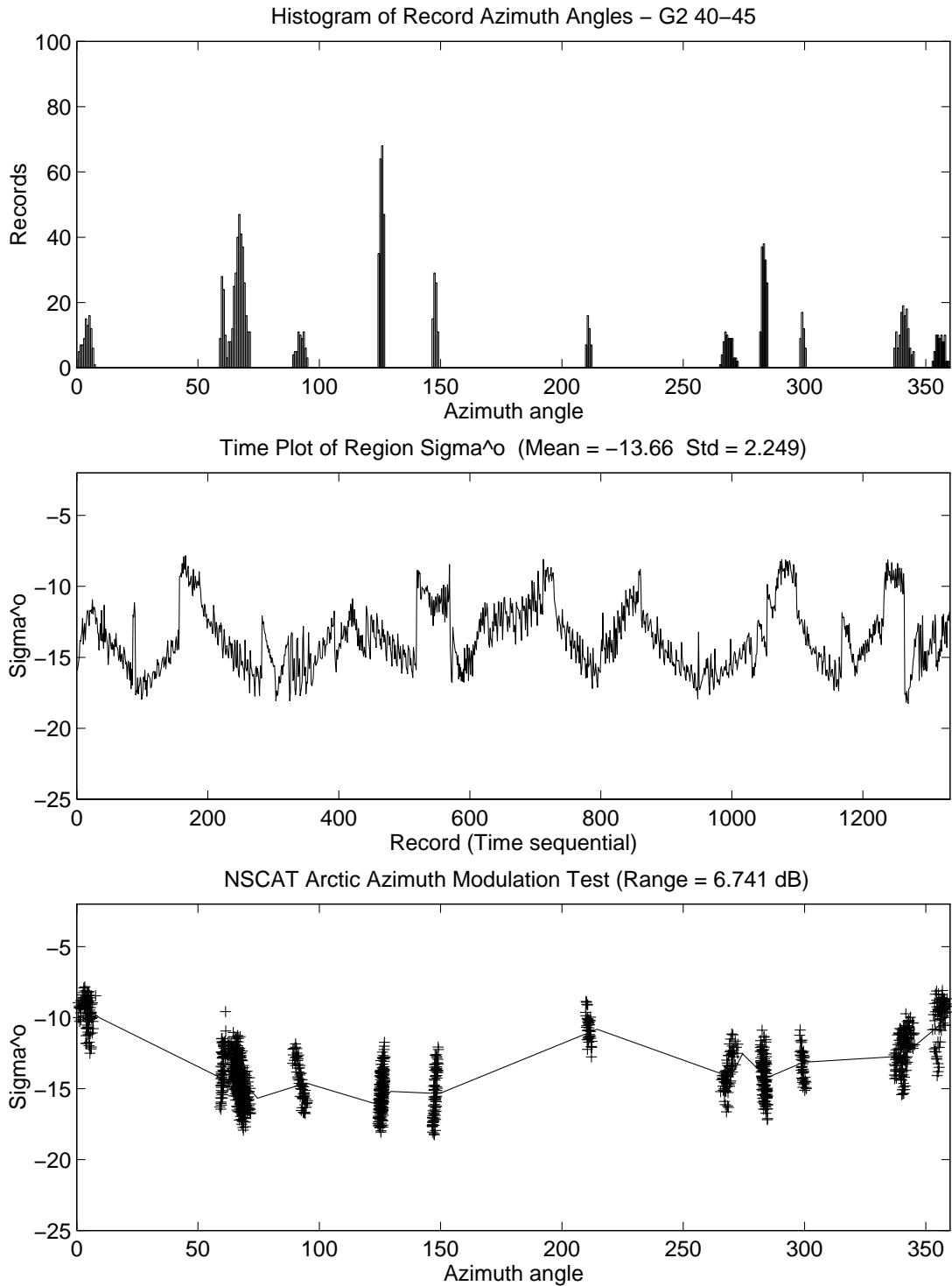


Figure 4: Plots illustrating the azimuth angle diversity,  $\sigma^o$  temporal dependence, and  $\sigma^o$  vs. azimuth angle for glacial ice region G2. All measurements have incidence angles in the range  $[40^\circ - 45^\circ]$ .

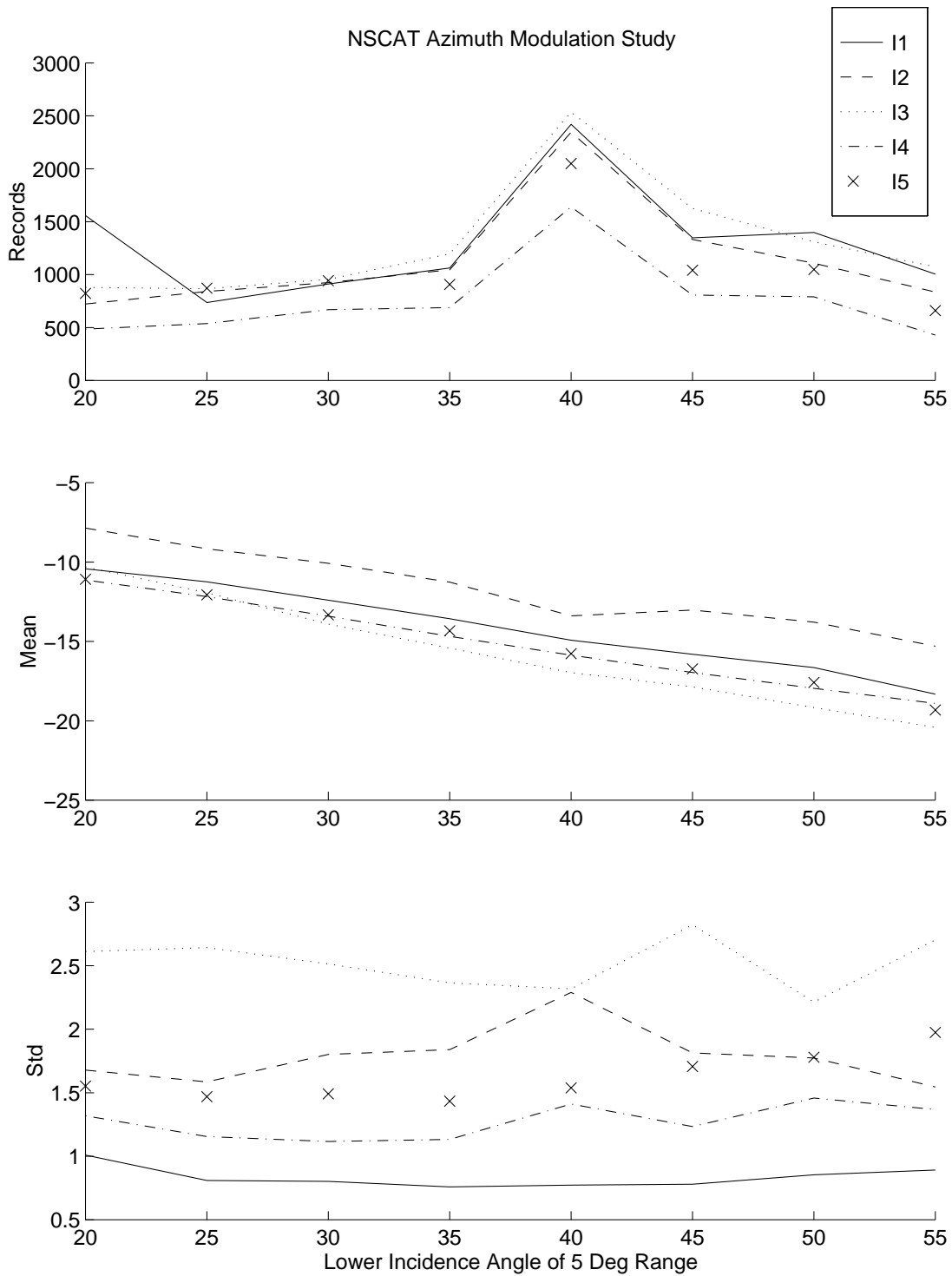


Figure 5: Plots of the number of records, mean  $\sigma^o$  value, and  $\sigma^o$  standard deviation values vs. incidence angle for sea ice regions 1-5.

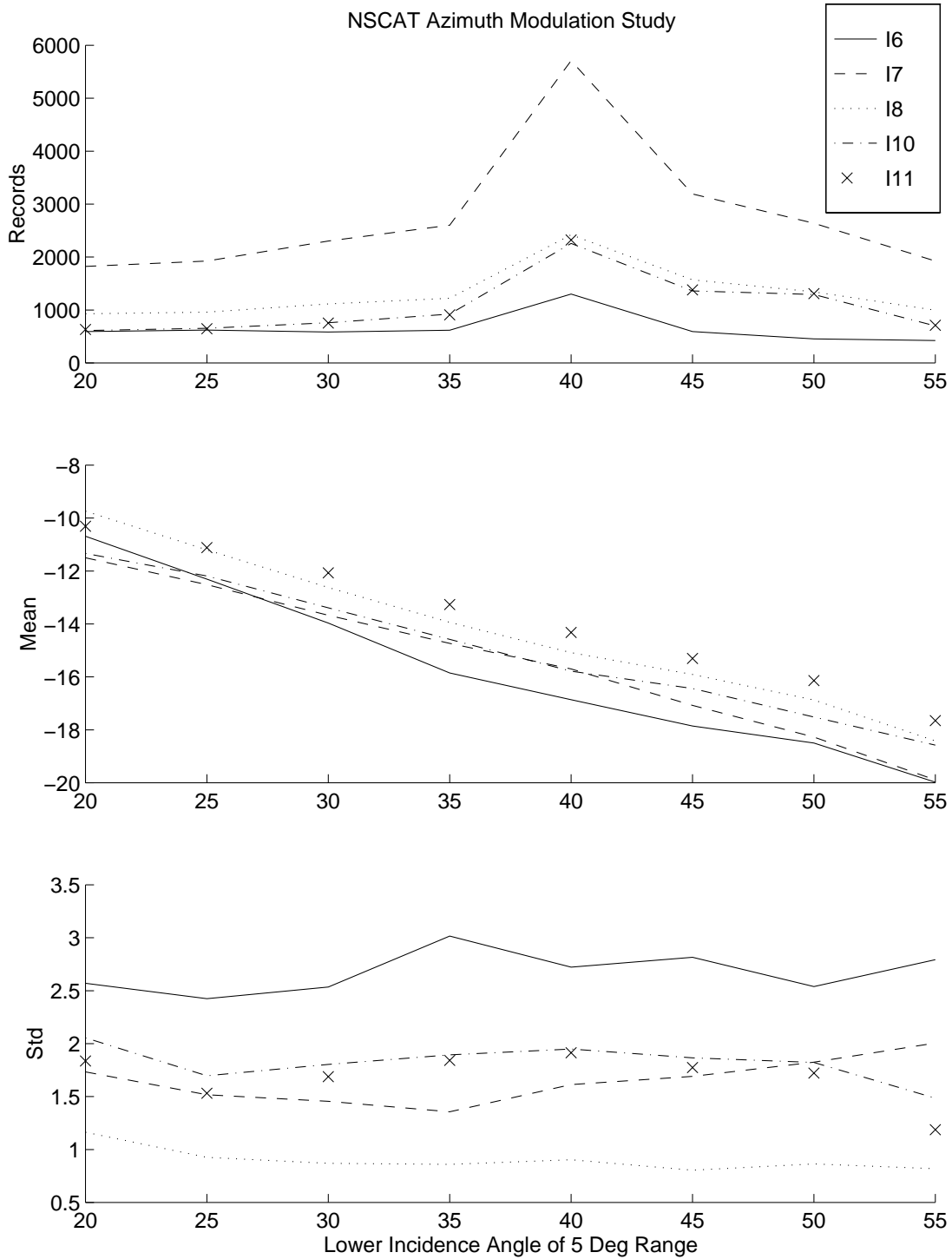


Figure 6: Plots of the number of records, mean  $\sigma^o$  value, and  $\sigma^o$  standard deviation values vs. incidence angle for sea ice regions 6-11.

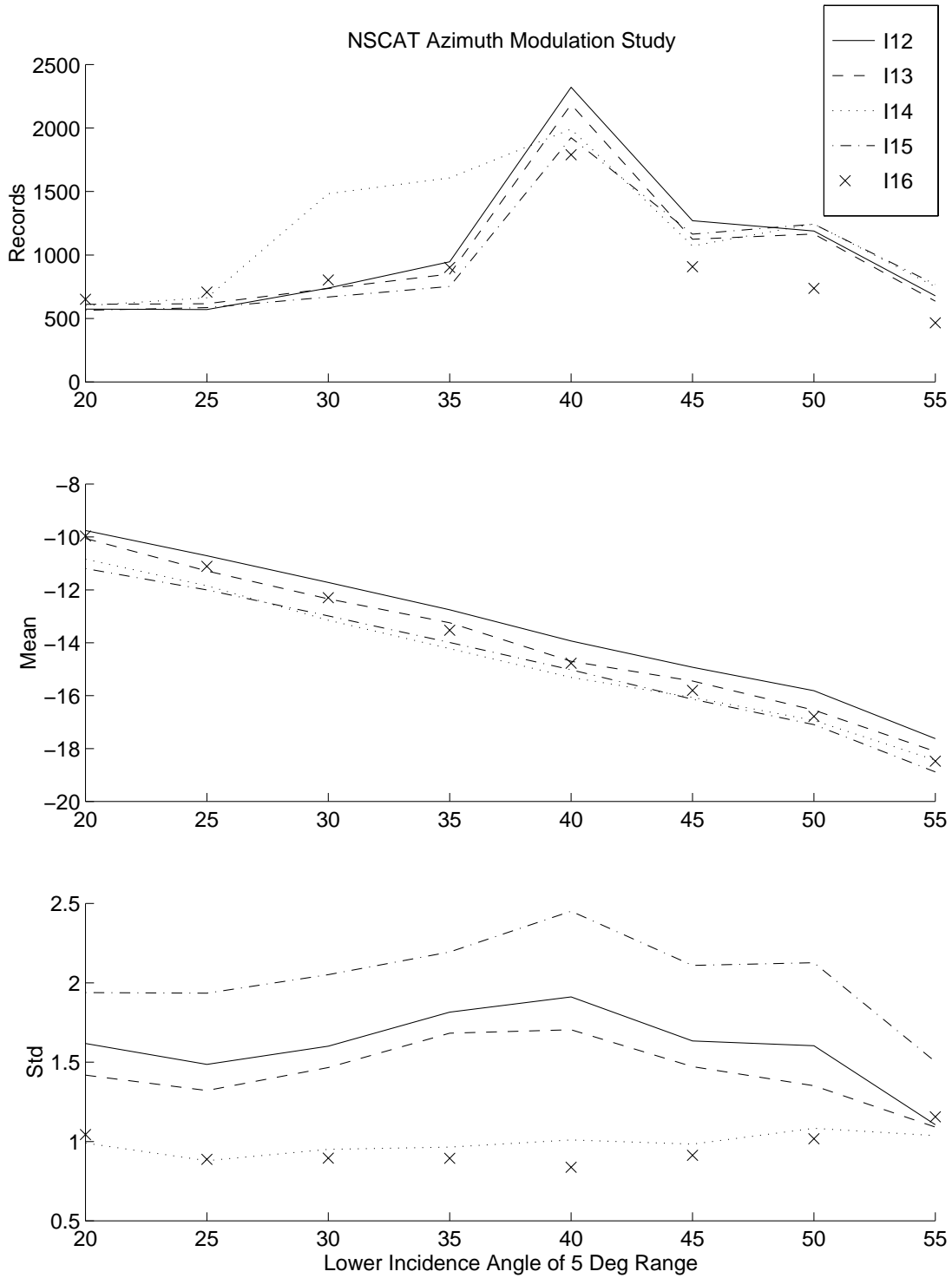


Figure 7: Plots of the number of records, mean  $\sigma^o$  value, and  $\sigma^o$  standard deviation values vs. incidence angle for sea ice regions 12-16.

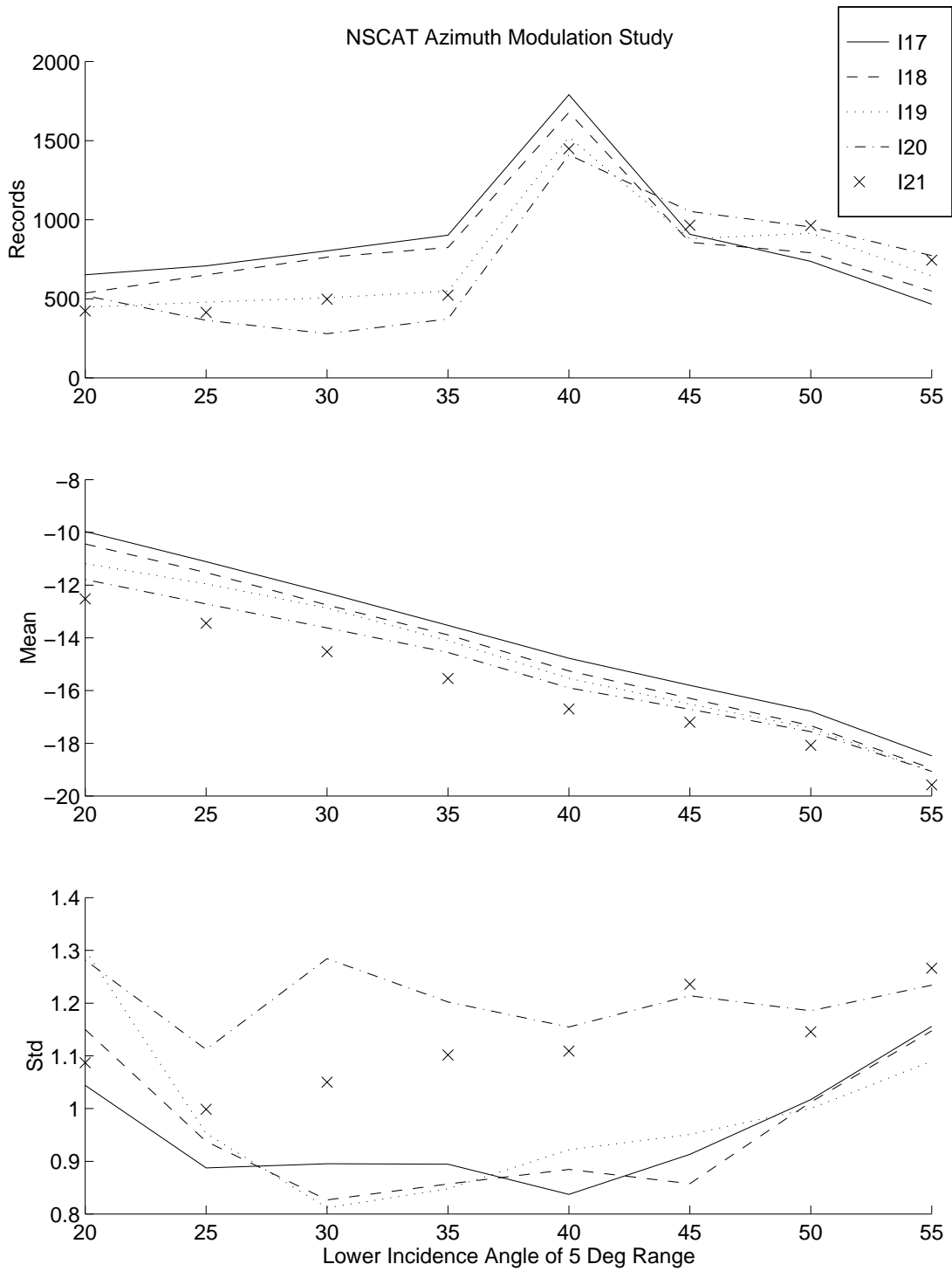


Figure 8: Plots of the number of records, mean  $\sigma^o$  value, and  $\sigma^o$  standard deviation values vs. incidence angle for sea ice regions 17-21.

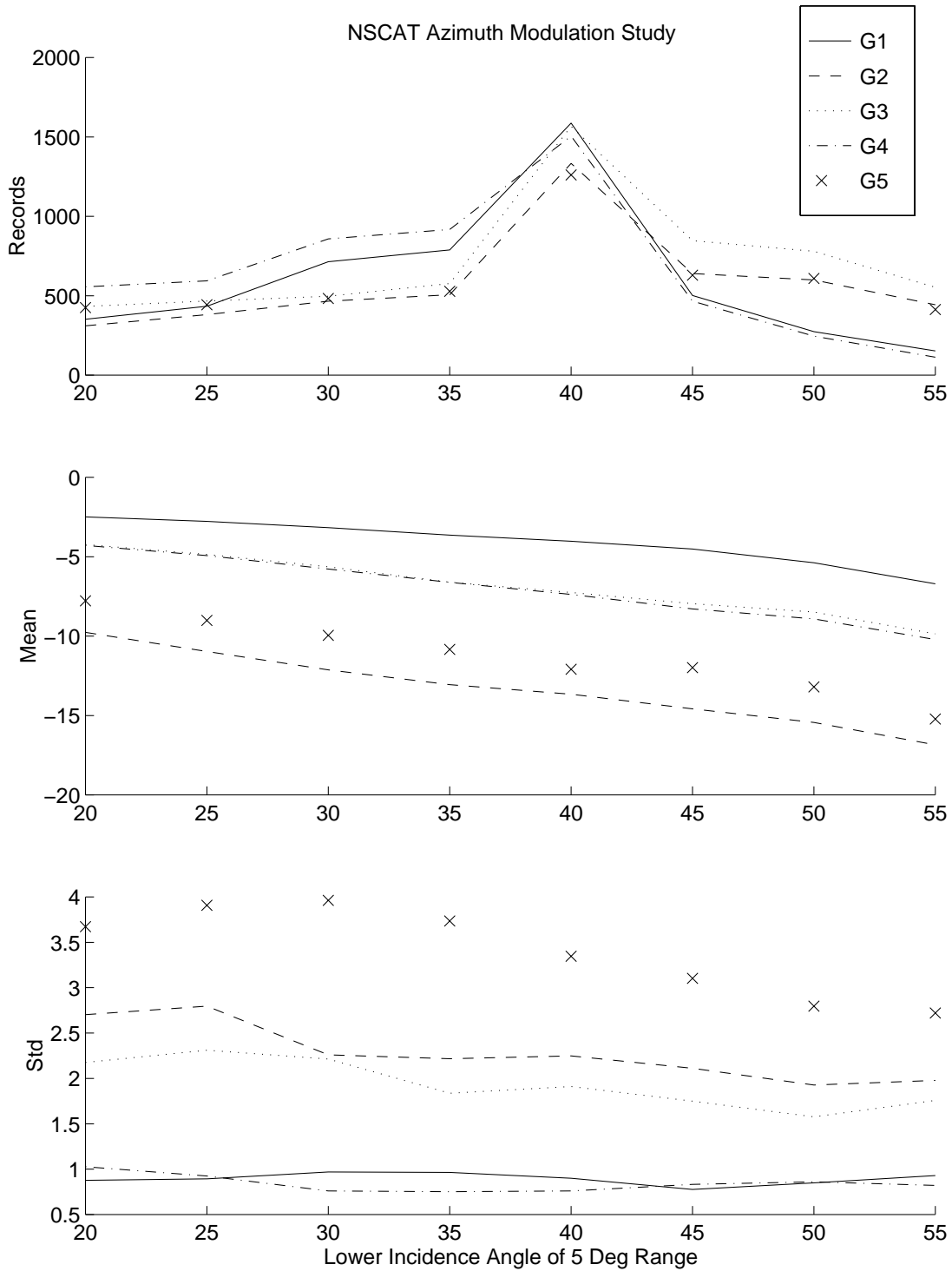


Figure 9: Plots of the number of records, mean  $\sigma^o$  value, and  $\sigma^o$  standard deviation values vs. incidence angle for glacial ice regions 1-5.

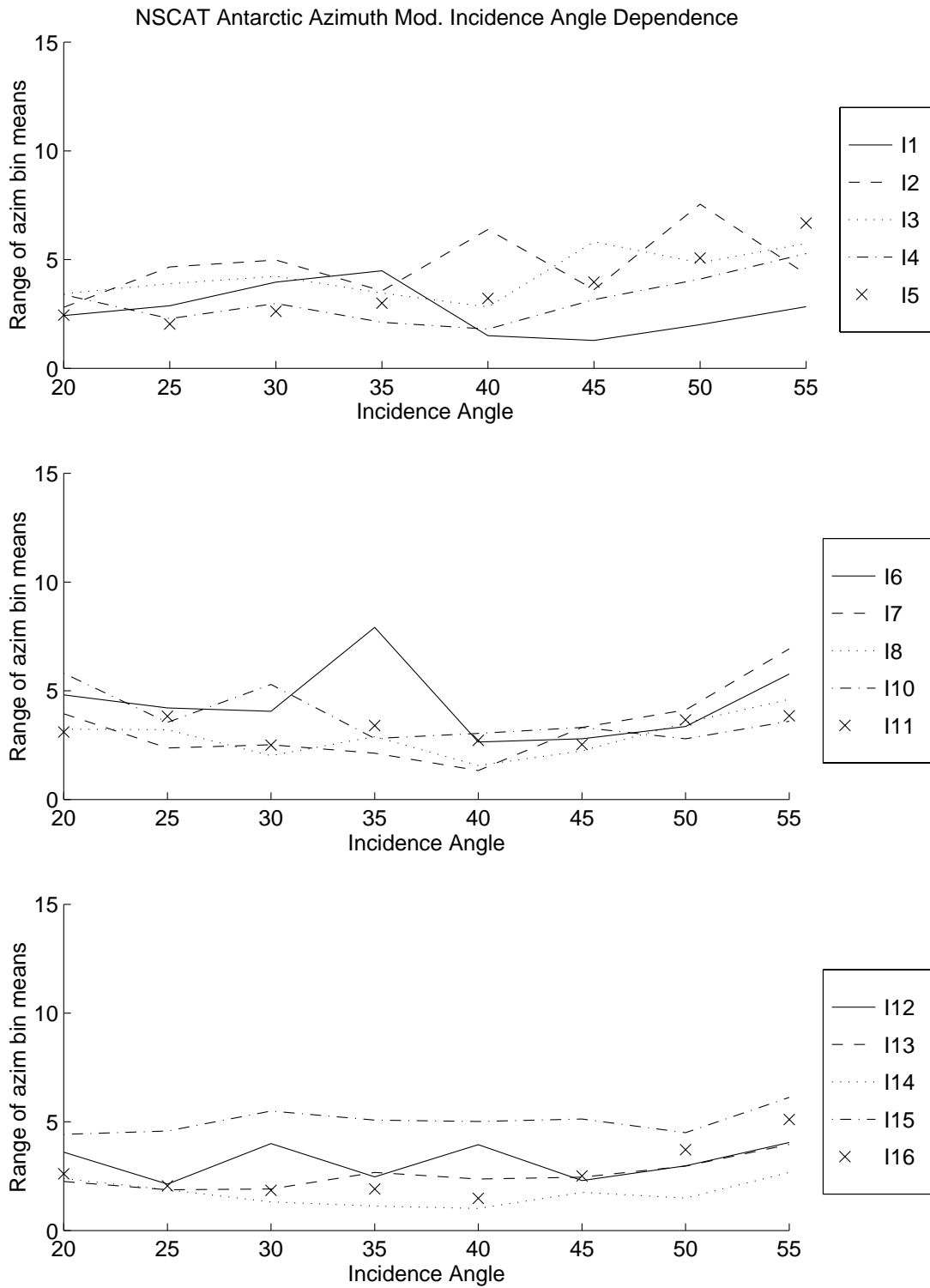


Figure 10: Plots of range of  $\sigma^0$  values at different azimuth angles vs. incidence angle for sea ice regions 1-16.

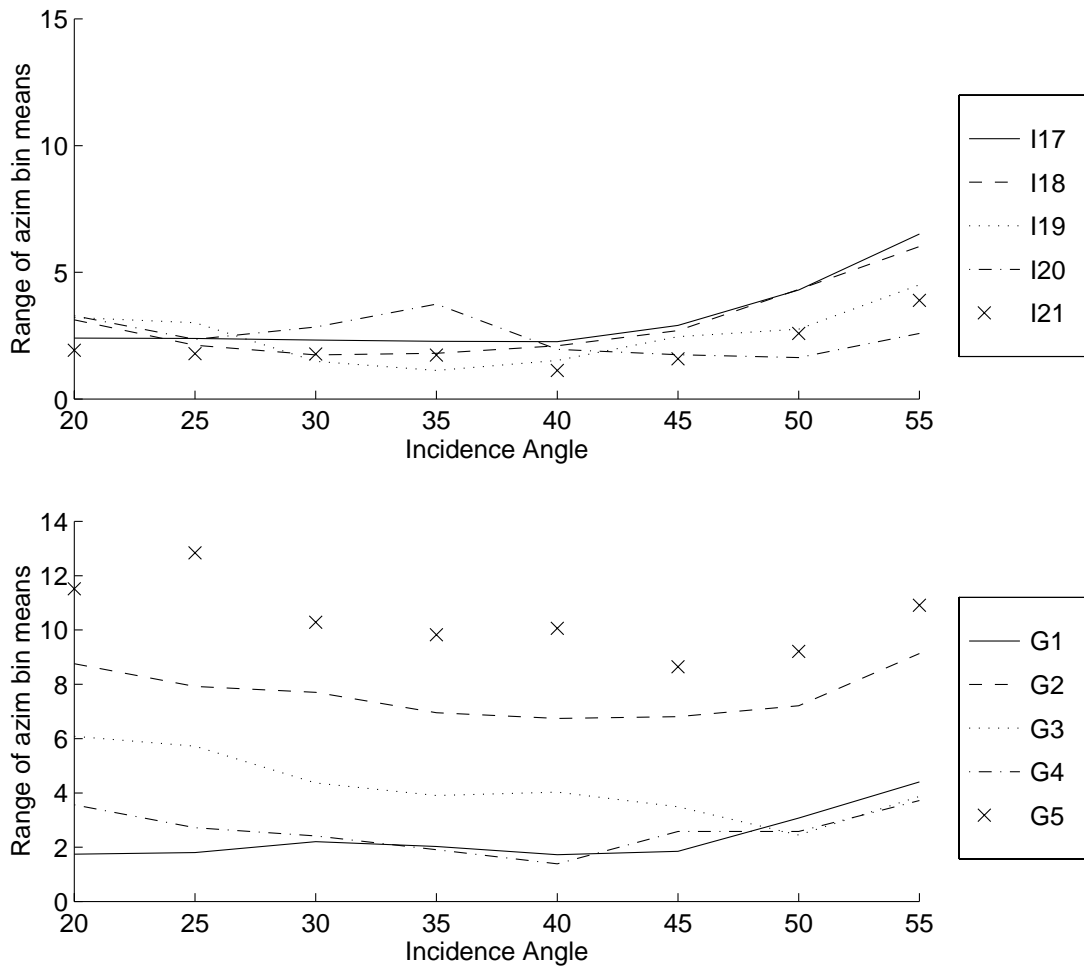


Figure 11: Plots of range of  $\sigma^o$  values at different azimuth angles vs. incidence angle for sea ice regions 17-21 and glacial regions 1-5.

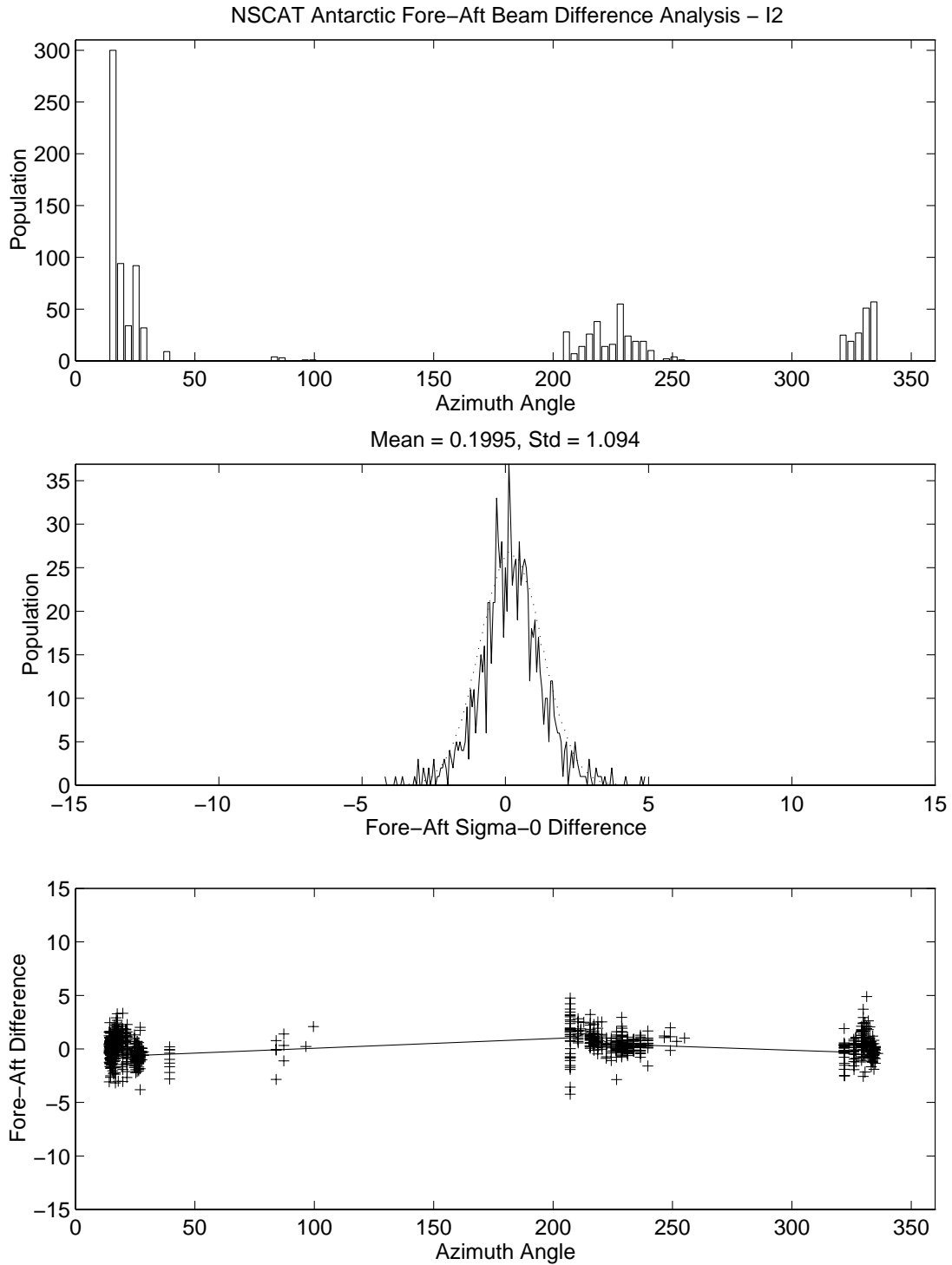


Figure 12: Plots illustrating azimuth angle diversity, the distribution of the fore-aft  $\sigma^0$  difference, and the fore-aft  $\sigma^0$  difference vs. azimuth angle for sea ice region I2. Note that the fore-aft  $\sigma^0$  difference is approximately zero-mean Gaussian indicating the absence of azimuth modulation.

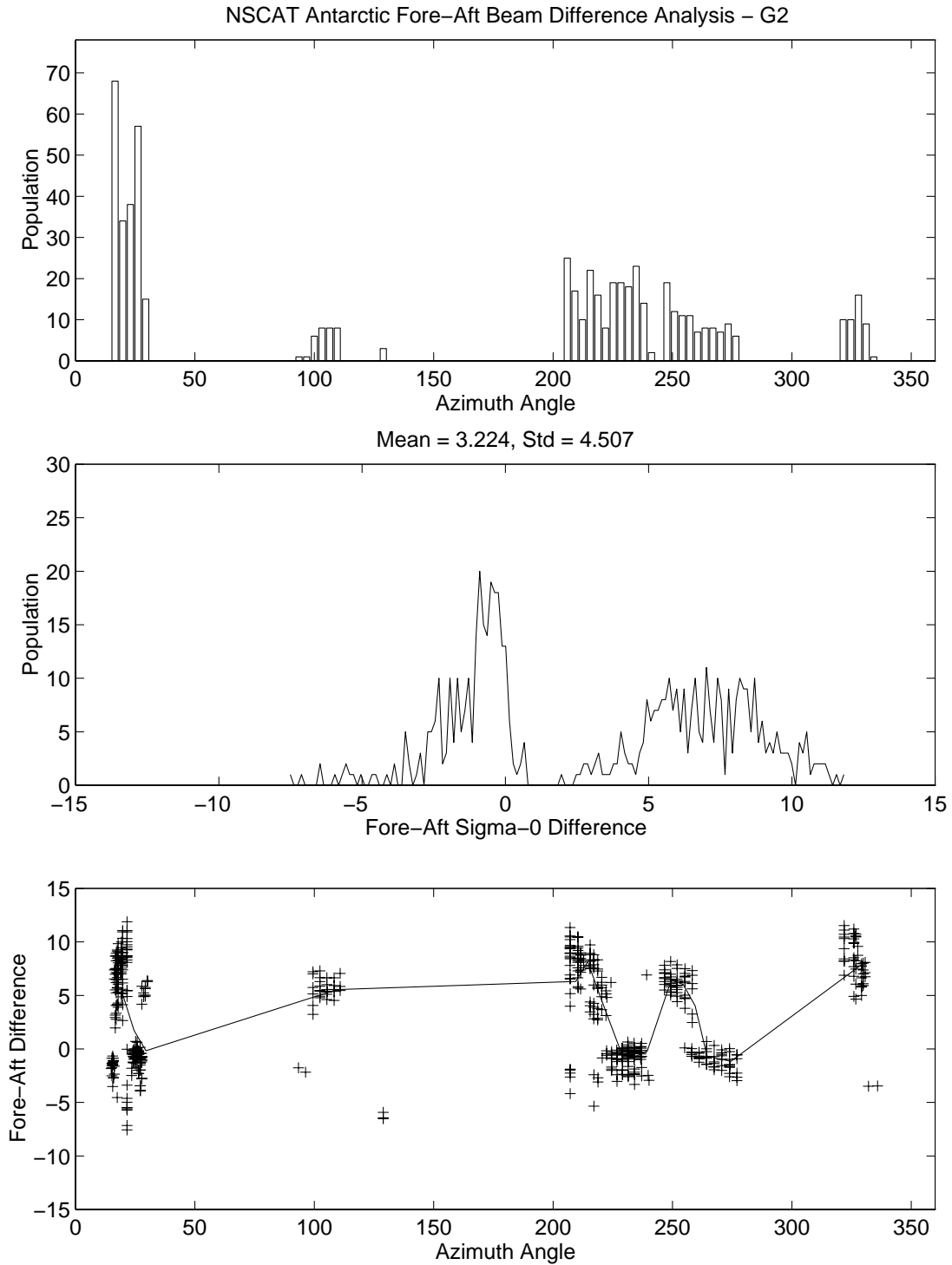


Figure 13: Plots illustrating azimuth angle diversity, the distribution of the fore-aft  $\sigma^0$  difference, and the fore-aft  $\sigma^0$  difference vs. azimuth angle for glacial ice region G2. Note that the fore-aft  $\sigma^0$  difference is not zero-mean Gaussian indicating the presence of azimuth modulation.

# Appendix A

# Appendix B